

Non-parallel vortex instability of natural convection flow over a non-isothermal horizontal flat plate

H. R. LEE, T. S. CHEN and B. F. ARMALY

Department of Mechanical and Aerospace Engineering and Engineering Mechanics,
University of Missouri-Rolla, Rolla, MO 65401, U.S.A.

(Received 16 November 1989 and in final form 2 March 1990)

Abstract—An analysis is performed to study the vortex instability of laminar boundary-layer flow in natural convection over a horizontal flat plate with variable surface temperature, $T_w(x) - T_\infty = Ax^n$. The analysis is based on the linear non-parallel flow model in which the steady main flow is treated as two-dimensional and account is taken of the streamwise dependence of the disturbance amplitude functions. Neutral stability curves as well as critical Grashof numbers and critical wave numbers are presented for Prandtl numbers of $0.7 \leq Pr \leq 100$, over a range of the exponent values n from $-1/3$ to 1.0 . For a given Prandtl number, the flow is found to become more stable to the vortex mode of instability as the value of the exponent n increases. However, fluids with a larger Prandtl number are found to be more susceptible to the instability than fluids with a lower Prandtl number. Results from the present non-parallel flow analysis are compared with available results from the parallel flow analyses and experiments. The streamwise variation of the disturbances is found to stabilize the flow.

INTRODUCTION

THE INSTABILITY of natural convection flow over inclined, upward-facing heated surfaces has been analyzed rather extensively (see, e.g. refs. [1-14]). From the experimental work of Lloyd and Sparrow [2] on natural convection flow in water over inclined heated plates, it was found that for inclination angles larger than 17° (relative to the vertical), the instability is characterized by the longitudinal vortex mode, whereas for inclination angles less than 14° the instability is characterized by the wave mode. In the range between 14° and 17° the two modes of instability were found to coexist. Their work has led to many analytical studies on the vortex instability for such a flow configuration.

In almost all of the analytical studies [3-6, 10, 11], a linear parallel flow model is employed, in which the disturbances are assumed to be invariable in the streamwise direction. This approximate analysis has provided critical Grashof numbers that are two to three orders of magnitude lower than those of experimental values. There is evidence from recent studies on vortex instability of forced convection flow [15-17] to indicate that the non-parallel flow analysis will yield more realistic predictions, when compared with experimental data, than those from the parallel flow analysis. This has motivated the present study.

In this study, the vortex instability of natural convection flow over a horizontal, upward-facing heated plate is analyzed by employing the non-parallel flow model in which account is taken of the streamwise variation of the disturbances. The surface temperature

of the plate is nonuniform and varies as $T_w(x) = T_\infty + Ax^n$. In the analysis, the disturbance quantities are properly scaled and the resulting partial differential equations for the disturbance amplitude functions, along with the boundary conditions, are converted into an eigenvalue problem which is solved numerically by an efficient finite-difference method [18] in conjunction with Müller's shooting procedure. Neutral stability curves as well as critical Grashof numbers and the corresponding critical wave numbers are presented for fluids with Prandtl numbers of $Pr = 0.7, 7, \text{ and } 100$ over a range of the exponent values, $-1/3 \leq n \leq 1$. The present results are also compared with previous results based on the parallel flow model and with available experimental data.

ANALYSIS

The main flow and thermal fields

As the first step in the analysis, attention is directed to the main flow and temperature fields. Consider a horizontal flat plate with its heated surface facing upward in a quiescent fluid at temperature T_∞ . The physical coordinates are chosen such that x is measured from the leading edge of the plate and y is measured normal to the plate. The surface temperature of the plate varies as $T_w(x) = T_\infty + Ax^n$ where A and the exponent n are real constants. Under the assumption of constant fluid properties and the use of the Boussinesq approximation, the main flow and thermal fields are governed by the following system of equations [19]:

NOMENCLATURE

u	dimensionless wave number of disturbance, $\alpha X^{-2/5}$	Greek symbols	
D	partial derivative with respect to η	α	dimensionless wave number of disturbances, $2\pi/\lambda$
f	reduced stream function, $\psi(x, y)/[5\nu(Gr_x/5)^{1/5}]$	$\tilde{\alpha}$	modified dimensionless wave number of disturbances corresponding to modified local Grashof number, $\{(6/5)^{1/6}[-\theta'(0)]^{-1/6}\}\alpha$
g	gravitational acceleration	β	volumetric coefficient of thermal expansion
Gr_x	local Grashof number, $g\beta[T_w(x) - T_\infty]x^3/\nu^2$	ε	dimensionless parameter, $(Gr_L/5)^{-1/5}$
\tilde{Gr}_x	modified local Grashof number, $g\beta q_w x^4/k\nu^2$	η	similarity variable, $(y/x)(Gr_x/5)^{1/5}$
Gr_L	Grashof number based on L , $g\beta[T_w(L) - T_\infty]L^3/\nu^2$	θ	dimensionless temperature, $(T - T_\infty)/[T_w(x) - T_\infty]$
k	thermal conductivity	κ	thermal diffusivity
L	characteristic length	λ	dimensionless wavelength
n	exponent in the power-law variation of the wall temperature	μ	dynamic viscosity
Nu_x	local Nusselt number	ν	kinematic viscosity
p'	disturbance pressure	ρ	density
P	mainflow pressure	τ_w	local wall shear stress
Pr	Prandtl number	ψ	stream function.
q_w	local surface heat flux		
t	dimensionless amplitude function of temperature disturbance		
t'	disturbance temperature		
T	mainflow temperature		
u, v, w	dimensionless amplitude functions of velocity disturbances in the x -, y -, z -directions, respectively		
u', v', w'	streamwise, normal, and spanwise components of disturbance velocity		
U, V	streamwise and normal velocity components of mainflow in the x -, y -directions, respectively		
x, y, z	streamwise, normal, and spanwise coordinates		
X, Y, Z	dimensionless streamwise, normal, and spanwise coordinates, defined, respectively, as x/L , $y/(\varepsilon L)$, and $z/(\varepsilon L)$.		
		Superscripts	
		+	dimensionless disturbance quantity
		-	scale quantity defined by equation (20)
		*	critical condition or dimensionless mainflow quantity
		~	resultant quantity.
		Subscripts	
		o	dimensionless amplitude function
		w	condition at wall
		∞	condition at free stream.

$$f''' + (n+3)ff'' - (2n+1)(f')^2 + \frac{1}{5} \left[(2-n)\eta\theta + (4n+2) \int_n^\infty \theta \, d\eta \right] = 0 \quad (1)$$

$$\theta'' + (n+3)Pr f\theta' - 5n Pr f'\theta = 0 \quad (2)$$

$$f(0) = f'(0) = f'(\infty) = \theta(\infty) = 0, \quad \theta(0) = 1 \quad (3)$$

where the similarity variable $\eta(x, y)$, the reduced stream function $f(\eta)$ and the dimensionless temperature $\theta(\eta)$ are defined, respectively, as

$$\begin{aligned} \eta &= (y/x)(Gr_x/5)^{1/5} \\ f(\eta) &= \psi(x, y)/[5\nu(Gr_x/5)^{1/5}] \\ \theta(\eta) &= (T - T_\infty)/[T_w(x) - T_\infty] \end{aligned} \quad (4)$$

with $Gr_x = g\beta[T_w(x) - T_\infty]x^3/\nu^2$ denoting the local Grashof number. In equations (1)–(3) the primes stand for differentiation with respect to η and Pr is the Prandtl number. Other notations are as defined in the Nomenclature.

Equations (1)–(3) were solved by an efficient finite-difference method [18] in conjunction with the cubic spline interpolation scheme to provide the main flow quantities that are needed in the instability calculations and to provide other physical quantities, such as the local Nusselt number Nu_x and the local wall shear stress τ_w . In terms of the dimensionless variables, the last two quantities can be expressed, respectively, by

$$\begin{aligned} Nu_x(Gr_x/5)^{-1/5} &= -\theta'(0) \\ \tau_w(x^2/5\mu\nu)(Gr_x/5)^{-3/5} &= f''(0). \end{aligned} \quad (5)$$

Formulation of the stability problem

In the stability analysis, the linear non-parallel-flow stability theory is employed. In experiments [1, 2] the vortex rolls have been found to be unchanging with time and periodic in the spanwise direction. Therefore, the disturbance quantities for velocity components u' , v' , w' , pressure p' and temperature t' are assumed to be a function of (x, y, z) , independent of time. These disturbance quantities are superimposed on the steady, two-dimensional main flow quantities U , V , $W = 0$, P , and T to obtain the following resultant quantities \hat{U} , \hat{V} , \hat{W} , \hat{P} , and \hat{T} :

$$\begin{aligned} \hat{U}(x, y, z) &= U(x, y) + u'(x, y, z) \\ \hat{V}(x, y, z) &= V(x, y) + v'(x, y, z) \\ \hat{W}(x, y, z) &= w'(x, y, z) \\ \hat{P}(x, y, z) &= P(x, y) + p'(x, y, z) \\ \hat{T}(x, y, z) &= T(x, y) + t'(x, y, z). \end{aligned} \quad (6)$$

Thus, the disturbance quantities are no longer considered to be independent of the streamwise coordinate x , as was done in previous studies. The resultant quantities given by equation (6) satisfy the continuity equation, Navier–Stokes equations, and energy equation for an incompressible, three-dimensional steady fluid flow. Substituting equation (6) into these equations, subtracting the two-dimensional main flow, and linearizing the disturbance quantities, one can arrive at the following disturbance equations:

$$\frac{\partial u'}{\partial x} + \frac{\partial v'}{\partial y} + \frac{\partial w'}{\partial z} = 0 \quad (7)$$

$$u' \frac{\partial U}{\partial x} + U \frac{\partial u'}{\partial x} + v' \frac{\partial U}{\partial y} + V \frac{\partial u'}{\partial y} = -\frac{1}{\rho} \frac{\partial p'}{\partial x} + \nu \nabla^2 u' \quad (8)$$

$$\begin{aligned} u' \frac{\partial V}{\partial x} + U \frac{\partial v'}{\partial x} + v' \frac{\partial V}{\partial y} + V \frac{\partial v'}{\partial y} \\ = -\frac{1}{\rho} \frac{\partial p'}{\partial y} + \nu \nabla^2 v' + g\beta t' \end{aligned} \quad (9)$$

$$U \frac{\partial w'}{\partial x} + V \frac{\partial w'}{\partial y} = -\frac{1}{\rho} \frac{\partial p'}{\partial z} + \nu \nabla^2 w' \quad (10)$$

$$u' \frac{\partial T}{\partial x} + U \frac{\partial t'}{\partial x} + v' \frac{\partial T}{\partial y} + V \frac{\partial t'}{\partial y} = \kappa \nabla^2 t' \quad (11)$$

where $\nabla^2 = \partial^2/\partial x^2 + \partial^2/\partial y^2 + \partial^2/\partial z^2$ is the Laplacian operator.

Since the disturbances are confined within the boundary layer of the main flow, the so-called bottling effect by Haaland and Sparrow [4], the disturbance equations will first be recast into the length scale of the main flow [12, 13]; that is

$$X = \frac{x}{L}, \quad Y = \frac{y}{\varepsilon L}, \quad \text{and} \quad Z = \frac{z}{\varepsilon L} \quad (12)$$

where $\varepsilon = (Gr_L/5)^{-1/5}$ and $Gr_L = g\beta[T_w(L) - T_\infty]L^3/\nu^2$ is the Grashof number based on the characteristic length $L(x)$. If $L = x$, then $Y = \eta$ and $Gr_L = Gr_x$. Other main flow quantities are scaled as

$$U^* = \frac{U\varepsilon^2 L}{\nu}, \quad V^* = \frac{V\varepsilon L}{\nu}, \quad \theta = \frac{T - T_\infty}{[T_w(x) - T_\infty]} \quad (13)$$

where U^* , V^* , and θ and their derivatives with respect to X and Y are of the order of 1. Similarly, the disturbance quantities can be scaled as

$$\begin{aligned} u^+ &= \frac{u'\varepsilon^2 L}{\nu}, \quad v^+ = \frac{v'\varepsilon^2 L}{\nu}, \quad w^+ = \frac{w'\varepsilon^2 L}{\nu}, \\ p^+ &= \frac{p'\varepsilon^3 L^2}{\mu\nu}, \quad t^+ = \frac{t'}{[T_w(x) - T_\infty]} \end{aligned} \quad (14)$$

where u^+ , v^+ , w^+ , p^+ , and t^+ and their derivatives with respect to X and Y are of the order of ε .

In terms of the above dimensionless variables, equations (7)–(11) become

$$\varepsilon \frac{\partial u^+}{\partial X} + \frac{\partial v^+}{\partial Y} + \frac{\partial w^+}{\partial Z} = 0 \quad (15)$$

$$\begin{aligned} u^+ \frac{\partial U^*}{\partial X} + U^* \frac{\partial u^+}{\partial X} + \frac{1}{\varepsilon} v^+ \frac{\partial U^*}{\partial Y} + V^* \frac{\partial u^+}{\partial Y} \\ = -\varepsilon \frac{\partial p^+}{\partial X} + \varepsilon^2 \frac{\partial^2 u^+}{\partial X^2} + \frac{\partial^2 u^+}{\partial Y^2} + \frac{\partial^2 u^+}{\partial Z^2} \end{aligned} \quad (16)$$

$$\begin{aligned} \varepsilon u^+ \frac{\partial V^*}{\partial X} + U^* \frac{\partial v^+}{\partial X} + v^+ \frac{\partial V^*}{\partial Y} + V^* \frac{\partial v^+}{\partial Y} \\ = -\frac{\partial p^+}{\partial Y} + \varepsilon^2 \frac{\partial^2 v^+}{\partial X^2} + \frac{\partial^2 v^+}{\partial Y^2} + \frac{\partial^2 v^+}{\partial Z^2} + \frac{5}{\varepsilon} t^+ \end{aligned} \quad (17)$$

$$\begin{aligned} U^* \frac{\partial w^+}{\partial X} + V^* \frac{\partial w^+}{\partial Y} = -\frac{\partial p^+}{\partial Z} \\ + \varepsilon^2 \frac{\partial^2 w^+}{\partial X^2} + \frac{\partial^2 w^+}{\partial Y^2} + \frac{\partial^2 w^+}{\partial Z^2} \end{aligned} \quad (18)$$

$$\begin{aligned} u^+ \frac{\partial \theta}{\partial X} + U^* \frac{\partial t^+}{\partial X} + \frac{v^+}{\varepsilon} \frac{\partial \theta}{\partial Y} + V^* \frac{\partial t^+}{\partial Y} \\ = \frac{1}{Pr} \left[\varepsilon^2 \frac{\partial^2 t^+}{\partial X^2} + \frac{\partial^2 t^+}{\partial Y^2} + \frac{\partial^2 t^+}{\partial Z^2} \right]. \end{aligned} \quad (19)$$

It is noted here that the term $(v^+/\varepsilon)\partial U^*/\partial Y$ in equation (16), the term $5t^+/\varepsilon$ in equation (17), and the term $(v^+/\varepsilon)\partial\theta/\partial Y$ in equation (19) are larger than the other terms in the corresponding equations by at least an order of $(1/\varepsilon)$. This means that the (X, Y, Z) variables as defined in equation (12) are not the appropriate length scales for the disturbances. Thus, by rescaling the coordinates for the disturbance quantities and the disturbance pressure in the form

$$(\bar{X}, \bar{Y}, \bar{Z}, \bar{p}^+) = (X, Y, Z, p^+) \varepsilon^{-1/2} \quad (20)$$

one arrives at

$$\varepsilon \frac{\partial u^+}{\partial \bar{X}} + \frac{\partial v^+}{\partial \bar{Y}} + \frac{\partial w^+}{\partial \bar{Z}} = 0 \quad (21)$$

$$\begin{aligned} \varepsilon u^+ \frac{\partial U^*}{\partial X} + \varepsilon^{1/2} U^* \frac{\partial u^+}{\partial \bar{X}} + v^+ \frac{\partial U^*}{\partial Y} + \varepsilon^{1/2} V^* \frac{\partial u^+}{\partial \bar{Y}} \\ = -\varepsilon^2 \frac{\partial \bar{p}^+}{\partial \bar{X}} + \varepsilon^2 \frac{\partial^2 u^+}{\partial \bar{X}^2} + \frac{\partial^2 u^+}{\partial \bar{Y}^2} + \frac{\partial^2 u^+}{\partial \bar{Z}^2} \end{aligned} \quad (22)$$

$$\begin{aligned} \varepsilon^2 u^+ \frac{\partial V^*}{\partial X} + \varepsilon^{1/2} U^* \frac{\partial v^+}{\partial \bar{X}} + \varepsilon v^+ \frac{\partial V^*}{\partial Y} + \varepsilon^{1/2} V^* \frac{\partial v^+}{\partial \bar{Y}} \\ = -\varepsilon \frac{\partial \bar{p}^+}{\partial \bar{Y}} + \varepsilon^2 \frac{\partial^2 v^+}{\partial \bar{X}^2} + \frac{\partial^2 v^+}{\partial \bar{Y}^2} + \frac{\partial^2 v^+}{\partial \bar{Z}^2} + 5t^+ \end{aligned} \quad (23)$$

$$\begin{aligned} \varepsilon^{1/2} U^* \frac{\partial w^+}{\partial \bar{X}} + \varepsilon^{1/2} V^* \frac{\partial w^+}{\partial \bar{Y}} = -\varepsilon \frac{\partial \bar{p}^+}{\partial \bar{Z}} \\ + \varepsilon^2 \frac{\partial^2 w^+}{\partial \bar{X}^2} + \frac{\partial^2 w^+}{\partial \bar{Y}^2} + \frac{\partial^2 w^+}{\partial \bar{Z}^2} \end{aligned} \quad (24)$$

$$\begin{aligned} \varepsilon u^+ \frac{\partial \theta}{\partial X} + \varepsilon^{1/2} U^* \frac{\partial t^+}{\partial \bar{X}} + v^+ \frac{\partial \theta}{\partial Y} + \varepsilon^{1/2} V^* \frac{\partial t^+}{\partial \bar{Y}} \\ = \frac{1}{Pr} \left[\varepsilon^2 \frac{\partial^2 t^+}{\partial \bar{X}^2} + \frac{\partial^2 t^+}{\partial \bar{Y}^2} + \frac{\partial^2 t^+}{\partial \bar{Z}^2} \right]. \end{aligned} \quad (25)$$

Since the terms $\varepsilon \partial u^+ / \partial \bar{X}$, $\varepsilon^2 \partial \bar{p}^+ / \partial \bar{X}$, $\varepsilon^2 \partial^2 u^+ / \partial \bar{X}^2$, $\varepsilon^2 \partial^2 v^+ / \partial \bar{X}^2$, $\varepsilon^2 \partial^2 w^+ / \partial \bar{X}^2$, and $\varepsilon^2 \partial^2 t^+ / \partial \bar{X}^2$ in equations (21)–(25) are smaller than the rest of the terms in their respective equations, these terms can be omitted. The omission of these lowest order terms in the disturbance equations is consistent with the level of approximation of the main flow. With the above-mentioned terms deleted and by making use of equation (20), the disturbance equations are reduced to

$$\frac{\partial v^+}{\partial \bar{Y}} + \frac{\partial w^+}{\partial \bar{Z}} = 0 \quad (26)$$

$$\begin{aligned} u^+ \frac{\partial U^*}{\partial X} + U^* \frac{\partial u^+}{\partial \bar{X}} + (Gr_L/5)^{1/5} v^+ \frac{\partial U^*}{\partial Y} \\ + V^* \frac{\partial u^+}{\partial \bar{Y}} = \frac{\partial^2 u^+}{\partial Y^2} + \frac{\partial^2 u^+}{\partial Z^2} \end{aligned} \quad (27)$$

$$\begin{aligned} (Gr_L/5)^{-1/5} u^+ \frac{\partial V^*}{\partial X} + U^* \frac{\partial v^+}{\partial \bar{X}} + v^+ \frac{\partial V^*}{\partial Y} + V^* \frac{\partial v^+}{\partial \bar{Y}} \\ = -\frac{\partial p^+}{\partial Y} + \frac{\partial^2 v^+}{\partial Y^2} + \frac{\partial^2 v^+}{\partial Z^2} + 5(Gr_L/5)^{1/5} t^+ \end{aligned} \quad (28)$$

$$U^* \frac{\partial w^+}{\partial X} + V^* \frac{\partial w^+}{\partial Y} = -\frac{\partial p^+}{\partial Z} + \frac{\partial^2 w^+}{\partial Y^2} + \frac{\partial^2 w^+}{\partial Z^2} \quad (29)$$

$$\begin{aligned} u^+ \frac{\partial \theta}{\partial X} + U^* \frac{\partial t^+}{\partial \bar{X}} + (Gr_L/5)^{1/5} v^+ \frac{\partial \theta}{\partial Y} \\ + V^* \frac{\partial t^+}{\partial \bar{Y}} = \frac{1}{Pr} \left[\frac{\partial^2 t^+}{\partial Y^2} + \frac{\partial^2 t^+}{\partial Z^2} \right]. \end{aligned} \quad (30)$$

Note that the main flow quantities, such as

U^* , $\partial U^* / \partial X$, $\partial U^* / \partial Y$, V^* , $\partial V^* / \partial X$, $\partial V^* / \partial Y$, $\partial \theta / \partial X$, and $\partial \theta / \partial Y$ can be expressed in terms of $f(\eta)$, $\theta(\eta)$ and their η derivatives. For example, $U^* = 5X^{1/5} f'(\eta)$, $V^* = -X^{-2/5} [3f(\eta) - 2\eta f'(\eta)]$, and $\partial \theta / \partial Y = X^{-2/5} \theta'(\eta)$.

Next, the pressure terms in equations (28) and (29) are eliminated by cross differentiation and subtraction. The resulting equation is then differentiated with respect to Z once and the substitution $\partial w^+ / \partial Z = -\partial v^+ / \partial Y$ from the continuity equation is employed to remove terms involving the function w^+ and its derivatives. This sequence of operations will yield three equations for the disturbance quantities u^+ , v^+ , and t^+ . For the non-parallel flow model considered here, these quantities are expressed as

$$(u^+, v^+, t^+) = [u_o(X, Y), v_o(X, Y), t_o(X, Y)] \exp(i\alpha Z) \quad (31)$$

where α is the dimensionless azimuthal wave number of the disturbances. Thus, the longitudinal vortex rolls are taken to be periodic in the spanwise Z -direction, with the amplitude functions depending on both X and Y .

Substituting equation (31) into equation (27), the combined form of equations (28) and (29) as described above, and equation (30), and letting

$$\alpha^2 = \alpha^2 X^{4/5}, \quad u = u_o, \quad v = v_o, \quad t = t_o X^{1/5} \quad (32)$$

one obtains the following system of partial differential equations for the disturbance amplitude functions u , v , and t :

$$D^2 u + a_1^* D u + a_2^* u + a_3^* v = 5f' X \frac{\partial u}{\partial X} \quad (33)$$

$$\begin{aligned} D^4 v + b_1^* D^3 v + b_2^* D^2 v + b_3^* D v + b_4^* v \\ + b_5^* u + b_6^* t = 5f' X \frac{\partial}{\partial X} (D^2 v) + 5f'' X \frac{\partial}{\partial X} (D v) \\ - 5\alpha^2 f' X \frac{\partial v}{\partial X} \end{aligned} \quad (34)$$

$$D^2 t + d_1^* D t + d_2^* t + d_3^* u + d_4^* v = 5Pr f' X \frac{\partial t}{\partial X} \quad (35)$$

along with boundary conditions

$$u = v = Dv = t = 0 \text{ at } \eta = 0 \text{ and } \infty \quad (36)$$

where

$$\begin{aligned} a_1^* &= 3f - 2\eta f', & a_2^* &= 2\eta f'' - f' - \alpha^2 \\ a_3^* &= -5f'' (Gr_x/5)^{1/5} \\ b_1^* &= 3f - 2\eta f', & b_2^* &= 5f' - 2\alpha^2 - 2\eta f'' \\ b_3^* &= 2f'' - 3\alpha^2 f + 2\alpha^2 \eta f', & b_4^* &= \alpha^4 + 2\alpha^2 \eta f'' - \alpha^2 f' \\ b_5^* &= \frac{2}{3} \alpha^2 (Gr_x/5)^{-1/5} (3f - \eta f' - 2\eta^2 f'') \\ b_6^* &= -5\alpha^2 (Gr_x/5)^{1/5} \\ d_1^* &= 3Pr f - 2Pr \eta f', & d_2^* &= Pr f' - \alpha^2 \\ d_3^* &= \frac{2}{3} Pr \eta \theta', & d_4^* &= -Pr \theta' (Gr_x/5)^{1/5}. \end{aligned} \quad (37)$$

In equations (33)–(36), D^j stands for the j th partial derivative with respect to η . Boundary conditions (36) arise from the fact that the disturbances vanish at the wall and in the free stream. The condition $Dv = 0$ results from the continuity equation (26) along with $w = 0$ at $\eta = 0$ and ∞ . For the case of weak X dependence, $\partial/\partial X \ll \partial/\partial \eta$ and the terms on the right-hand side of equations (33)–(35) can be deleted. The resulting equations along with boundary conditions (36) then provide a system of equations that closely resemble those for the case of the parallel flow model in which the amplitude functions u , v , and t depend only on the Y or η coordinate.

Since equations (33)–(35) are partial differential equations, the boundary conditions given by equation (36) are not sufficient if the X derivative of u , v , and t are not to be set arbitrarily equal to zero. To define the problem completely, one needs to specify the initial conditions for u , v , and t at an upstream location $X = X_1$. However, for the problem considered here, the terms involving $X \partial/\partial X$ can be related to $\eta \partial/\partial \eta$ by the coordinate transformation

$$X \frac{\partial}{\partial X} = X \frac{\partial}{\partial \eta} \frac{\partial \eta}{\partial X} = -\frac{2}{5} \eta \frac{\partial}{\partial \eta}. \quad (38)$$

With this, equations (33)–(35) reduce to ‘ordinary differential equations’ as follows:

$$D^2 u + a_1 D u + a_2 u + a_3 v = 0 \quad (39)$$

$$D^4 v + b_1 D^3 v + b_2 D^2 v + b_3 D v + b_4 v + b_5 u + b_6 t = 0 \quad (40)$$

$$D^2 t + d_1 D t + d_2 t + d_3 u + d_4 v = 0. \quad (41)$$

Equations (39)–(41) along with boundary conditions (36), represent the mathematical system for the instability problem. In these equations

$$a_1 = a_1^* + 2\eta f', \quad a_2 = a_2^*, \quad a_3 = a_3^*$$

$$b_1 = b_1^* + 2\eta f', \quad b_2 = b_2^* + 2\eta f'', \quad b_3 = b_3^* - 2\alpha^2 \eta f'$$

$$b_4 = b_4^*, \quad b_5 = b_5^*, \quad b_6 = b_6^*$$

$$d_1 = d_1^* + 2Pr \eta f', \quad d_2 = d_2^*$$

$$d_3 = d_3^*, \quad d_4 = d_4^*. \quad (42)$$

The system of coupled differential equations, equations (39)–(41), along with boundary conditions (36), constitutes an eigenvalue problem of the form

$$E(\alpha, Gr_x; Pr, n) = 0. \quad (43)$$

In determining the neutral stability curves for given values of the exponent n and the Prandtl number Pr , the value of Grashof number, Gr_x , satisfying equation (43) is sought as the eigenvalue for a prescribed value of the wave number α .

NUMERICAL METHOD OF SOLUTIONS

The system of equations for the main flow and thermal fields, equations (1)–(3), was solved by a finite-

difference scheme in conjunction with a cubic spline interpolation procedure similar to, but modified from that described in ref. [18] to provide the main flow quantities f , f' , f'' , θ , and θ' that are needed in the stability computation and in the determination of the local Nusselt number and the local wall shear stress. The stability problem, consisting of equations (39)–(41) and (36), was solved by a finite-difference scheme along with Müller’s shooting method. The solution method parallels that described in ref. [18] and to conserve space it is not repeated here. It suffices to mention some of its highlights. Equations (2) and (41) will become stiff when the Prandtl number is very large. To solve stiff differential equations by the finite-difference method, an upwind scheme or its equivalent is required. In the present study, a finite-difference method based on a weighting function scheme [18] was used. This numerical method enables the scheme to shift automatically from the central difference algorithm to the upwind-difference algorithm, and vice versa. Furthermore, to proceed with the numerical calculation of the stability problem, the boundary conditions at $\eta = \eta_\infty$ need to be approximated by the asymptotic solutions of equations (39)–(41) at $\eta = \eta_\infty$ (i.e. at the edge of the boundary layer). Since $f' = f'' = \theta = \theta' = 0$ at $\eta = \eta_\infty$, the asymptotic solutions for u , v , and t at $\eta = \eta_\infty$ can be obtained as

$$u_2 = \exp(-m\eta_\infty), \quad u_1 = u_3 = u_4 = 0$$

$$v_1 = \exp(-\alpha\eta_\infty), \quad v_2 = \exp(-m\eta_\infty)$$

$$v_3 = \exp(-r\eta_\infty), \quad v_4 = \eta_\infty \exp(-m\eta_\infty)$$

$$t_3 = \exp(-r\eta_\infty), \quad t_1 = t_2 = t_4 = 0 \quad (44)$$

where

$$r = \{-C Pr + [(C Pr)^2 + 4\alpha^2]^{1/2}\}/2$$

$$m = \{-C + [C^2 + 4\alpha^2]^{1/2}\}/2 \quad (45)$$

with $C = -3f$.

At any η location, the solutions for u , v , and t are

$$u(\eta) = K_1 u_1(\eta) + K_2 u_2(\eta) + K_3 u_3(\eta) + K_4 u_4(\eta)$$

$$v(\eta) = K_1 v_1(\eta) + K_2 v_2(\eta) + K_3 v_3(\eta) + K_4 v_4(\eta)$$

$$t(\eta) = K_1 t_1(\eta) + K_2 t_2(\eta) + K_3 t_3(\eta) + K_4 t_4(\eta) \quad (46)$$

where K_1 , K_2 , K_3 , and K_4 are constants.

With a preassigned value of n , the main flow solution is first obtained for a fixed Prandtl number, Pr . Next, with the wave number α specified and a guessed value of the local Grashof number Gr_x as the eigenvalue, the finite-difference form of equations (39)–(41) and (36) is numerically solved from $\eta = 0$ to η_∞ , ending with the asymptotic solutions for u , v , and t at $\eta = \eta_\infty$. The guessed eigenvalue Gr_x is then corrected by Müller’s shooting method until the boundary conditions at the wall ($\eta = 0$) are satisfied within a certain specified tolerance. This yields a converged Gr_x value as the eigenvalue for given values of n , Pr , and α .

After some experiments with the numerical solu-

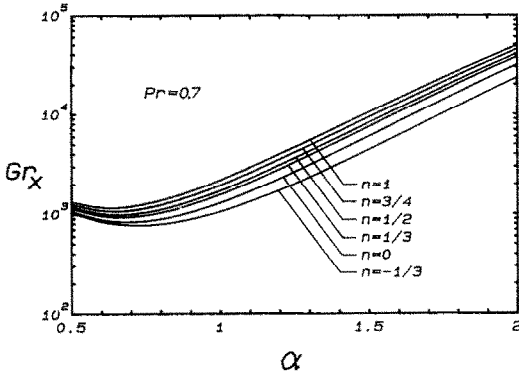


FIG. 1. The effect of n on neutral stability curves for $Pr = 0.7$.

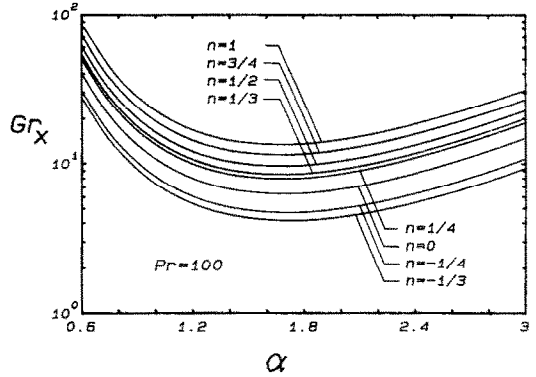


FIG. 3. The effect of n on neutral stability curves for $Pr = 100$.

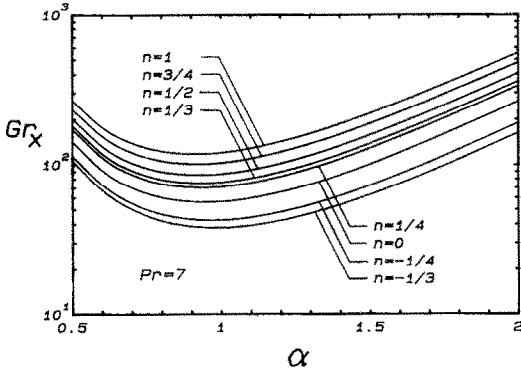


FIG. 2. The effect of n on neutral stability curves for $Pr = 7$.

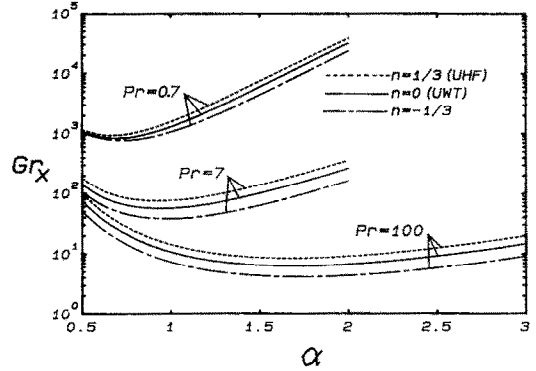


FIG. 4. The effect of Pr on the neutral stability curves for $n = -1/3, 0$ (UWT), and $1/3$ (UHF).

tions, a step size of $\Delta\eta = 0.005$ and a value of $\eta_\infty = 10$ were found to be sufficient for both the main flow and stability calculations for $Pr = 7$ and 100 . However, a step size of $\Delta\eta = 0.005$ and a value of $\eta_\infty = 20$ were needed for $Pr = 0.7$ to provide accurate numerical results for both. It is also worth noting from the numerical experiments that a smaller step size in $\Delta\eta$ is found to be more important than a larger value of η_∞ . This is especially true when the wave number α is small.

RESULTS AND DISCUSSION

To determine the stability and instability domains and the critical Grashof number (i.e. the minimum Grashof numbers for the incipency of the vortex instability), neutral stability curves (i.e. the Grashof number vs wave number curves) were obtained. The neutral stability curves for different values of the exponent n , ranging from $-1/3$ to 1 , are plotted in Figs. 1–3 separately for Prandtl numbers Pr of $0.7, 7$, and 100 . It can be seen from these figures that the flow becomes less susceptible to the vortex instability as the value of exponent n increases. Representative neutral stability curves for $n = -1/3, 0$ (the uniform wall temperature, UWT, case), and $1/3$ (the uniform surface heat flux, UHF, case) are compared in Fig. 4 for $Pr = 0.7, 7$, and 100 . It shows that the instability

is enhanced as Pr increases. The critical Grashof numbers and the corresponding critical wave numbers, along with the local Nusselt number $Nu_x (Gr_x/5)^{-1/5} = -\theta'(0)$ and the local shear stress $\tau_w (x^2/5\mu\nu) (Gr_x/5)^{-3/5} = f''(0)$, for different values of n and Pr are listed in Table 1.

Figure 5 shows the critical Grashof number and the critical wave number as a function of the exponent n for different Prandtl numbers. An inspection of Table 1 and Fig. 5 reveals that for a given value of the exponent n , the critical Grashof number decreases with an increase in the Prandtl number, Pr . However, for a given Prandtl number, the critical Grashof numbers for $n > 0$ are larger than that for the case of $n = 0$ (the UWT case), but are smaller when $n < 0$. This trend can also be observed in Figs. 1–3, which implies that the flow will become less susceptible to the vortex instability as the value of n increases. This is to be expected, because when $n = 0$ there is a step jump in the temperature difference $(T_w - T_\infty) = A$ at $x = 0$ for all x , whereas for $n > 0$ the wall temperature starts with $T_w = T_\infty$ at $x = 0$ and increases with x , and for $n < 0$ it starts with $T_w \rightarrow \infty$ at $x = 0$ and decreases with x . Thus, for $n < 0$ a larger jump in $(T_w - T_\infty)$ occurs at a smaller x than for $n = 0$. This contributes to an earlier onset of the instability and hence a smaller critical Grashof number. This same trend was also

Table 1. Critical Grashof number, critical wave number, local Nusselt number and local wall shear stress

<i>n</i>	<i>Pr</i> = 0.7				<i>Pr</i> = 7				<i>Pr</i> = 100			
	Gr_x^*	α^*	$-\theta'(0)$	$f''(0)$	Gr_x^*	α^*	$-\theta'(0)$	$f''(0)$	Gr_x^*	α^*	$-\theta'(0)$	$f''(0)$
1	1164.8	0.62066	0.82703	0.60159	117.70	0.90566	1.39955	0.23950	13.470	1.6635	2.45011	0.08387
3/4	1075.5	0.63690	0.76234	0.58415	100.99	0.91200	1.29837	0.23426	11.502	1.6641	2.27896	0.08240
1/2	989.56	0.65379	0.68840	0.56483	85.252	0.91887	1.18280	0.22884	9.6599	1.6654	2.08333	0.08099
1/3	933.99	0.66405	0.63186	0.55074	75.264	0.92484	1.09432	0.22525	8.4967	1.6675	1.93332	0.08015
1/4	907.65	0.67004	0.60063	0.54331	70.411	0.92839	1.04535	0.22351	7.9327	1.6691	1.85018	0.07979
0	834.52	0.68803	0.48933	0.51945	56.326	0.94275	0.86956	0.21904	6.2972	1.6775	1.55059	0.07924
-1/4	780.19	0.70939	0.32818	0.49431	42.616	0.96876	0.60739	0.21819	4.6925	1.6978	1.09815	0.08076
-1/3	771.92	0.72046	0.25067	0.48657	37.951	0.98318	0.47532	0.22026	4.1372	1.7111	0.86632	0.08251

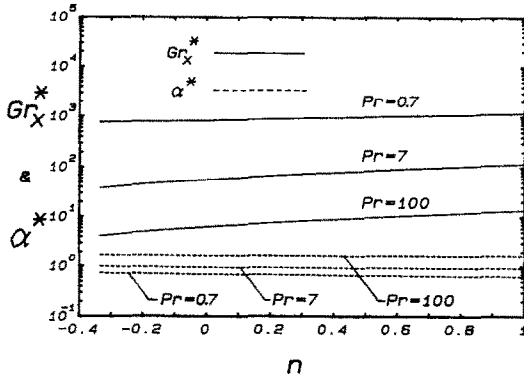


FIG. 5. Critical values of Grashof number and wave number for $Pr = 0.7, 7, 100$, and $-1/3 \leq n \leq 1$.

observed in the work of refs. [12, 13]. One can also see from Fig. 5 that for a given value of the exponent n , the critical wave number increases with increasing Prandtl number, Pr . This trend is similar to that found in earlier analytical [4, 5] and experimental [9] studies. Figure 5 also shows that in the linear-logarithm scale the critical Grashof number increases almost linearly with an increase in the exponent value n , whereas the critical wave number decreases linearly with n .

In order to compare directly the critical Grashof number and the critical wave number from the present analysis based on the non-parallel flow model with those from the analysis by the parallel flow model for the UHF case reported in ref. [11], one needs to define an equivalent Grashof number and an equivalent wave number. The case of $n = 1/3$ corresponds to the UHF case. It can be shown that

$$Gr_x = 5^{1/6}[-\theta'(0)]^{-5/6} \tilde{Gr}_x^{5/6} \tag{47}$$

$$\alpha = (5/6)^{1/6}[-\theta'(0)]^{1/6} \tilde{\alpha} \tag{48}$$

where $\tilde{Gr}_x = g\beta q_w x^4 / kv^2$ and $\tilde{\alpha}$ are, respectively, the modified Grashof number and wave number for the UHF case. In Table 2 a comparison of the critical values is made between the present non-parallel flow model and the parallel flow model and with available experimental data [14]. From the table one can see that the critical Grashof numbers from the non-parallel flow model are much larger than those from the parallel flow model for both $Pr = 0.7$ and 7 . That is, the more rigorous non-parallel flow analysis, which

takes into account the streamwise dependence of the disturbances, predicts a more stable flow condition than that predicted by the parallel flow model and hence the results are in better agreement with available experimental data. However, the difference in the critical Grashof numbers between the prediction and the experiment is still very large. It should be noted that the present prediction is based on the linear theory in which the disturbance quantities are assumed to be infinitesimally small. In real situations, natural disturbances in boundary layer flow need to be amplified before they can be detected. Thus, to remedy the discrepancy in the results between the linear theory and experiments, further analytical studies are needed. They may include a linear analysis by considering also the time dependence of the amplitude functions or a non-linear analysis, which are being attempted by the authors.

Because no experiments on the vortex instability of natural convection flow over a horizontal flat plate are available for the power-law wall temperature variation except for the UWT case ($n = 0$), the results from the present analysis for $n \neq 0$ cannot be verified directly with experimental results.

CONCLUSION

In this paper vortex instability of laminar boundary layer flow in natural convection over a horizontal flat plate has been analyzed for non-isothermal wall temperatures by employing the linear non-parallel flow theory. Critical Grashof numbers are presented for $Pr = 0.7, 7$, and 100 over a range of the exponent values n from $-1/3$ to 1 . The major findings from the present study are: (1) for a given value of Prandtl number Pr , the critical Grashof number increases with increasing value of the exponent n , (2) for a given value of the exponent n , the critical Grashof number decreases with increasing Prandtl number, and (3) the non-parallel flow analysis provides a larger critical Grashof number than the parallel flow analysis, thus bringing the prediction closer to available experimental data. However, the discrepancy between results from the theory and experiments is still large.

Acknowledgement—Part of the numerical results reported in this paper was obtained by using a Cray X-MP Super-

Table 2. A comparison of Gr_x^* and α^* between non-parallel flow model and parallel flow model and with available experimental data

Gr_x^* α^*	$Pr = 0.7$				$Pr = 7$				
	Non-parallel flow $n = 0$	Parallel flow UWT [10]	Experiments UWT Cheng and Kim [14]	Non-parallel flow $n = 1/3$	Parallel flow UHF [11]	Non-parallel flow $n = 0$	Parallel flow UWT [10]	Non-parallel flow $n = 1/3$	Parallel flow UHF [11]
834.52 0.68803		340 0.583	6.35 ~ 11.37 × 10 ⁵ 0.33204 ~ 0.42970	933.99 0.66405	230.72 0.53288	56.326 0.94275	22 0.825	75.264 0.92484	14.185 0.76712

computer through the facility of the National Center for Supercomputing Applications (NCSA) at the University of Illinois.

REFERENCES

1. E. M. Sparrow and R. B. Husar, Longitudinal vortices in natural convection flow on inclined surfaces, *J. Fluid Mech.* **37**, 251–255 (1969).
2. J. R. Lloyd and E. M. Sparrow, On the instability of natural convection flow on inclined plates, *J. Fluid Mech.* **42**, 465–470 (1970).
3. G. J. Hwang and K. C. Cheng, Thermal instability of laminar natural convection flow on inclined isothermal plates, *Can. J. Chem. Engng* **51**, 659–666 (1973).
4. S. E. Haaland and E. M. Sparrow, Vortex instability of natural convection flow on inclined surfaces, *Int. J. Heat Mass Transfer* **16**, 2355–2367 (1973).
5. R. A. Kahawita and R. N. Meroney, The vortex mode of instability in natural convection flow along inclined plates, *Int. J. Heat Mass Transfer* **17**, 541–548 (1974).
6. P. A. Iyer and R. E. Kelly, The instability of the laminar free convection flow induced by a heated inclined plate, *Int. J. Heat Mass Transfer* **17**, 517–525 (1974).
7. G. S. H. Lock, C. Gort and G. R. Pond, A study of instability in free convection from an inclined plate, *Appl. Scient. Res.* **18**, 171–182 (1967).
8. D. T. Tritton, Transition to turbulence in the free convection boundary layers on an inclined heated plate, *J. Fluid Mech.* **16**, 417–435 (1963).
9. J. R. Lloyd, Vortex wavelength in the transition flow adjacent to upward facing inclined isothermal surfaces, *Proc. 5th Int. Heat Transfer Conf.*, Vol. III, Paper No. NCL 8, pp. 34–37 (1974).
10. T. S. Chen and K. L. Tzuoo, Vortex instability of free convection flow over horizontal and inclined surfaces, *J. Heat Transfer* **104**, 637–643 (1982).
11. H. C. Tien, T. S. Chen and B. F. Armaly, Vortex instability of natural convection flow over horizontal and inclined plates with uniform surface heat flux, *Numer. Heat Transfer* **9**, 697–713 (1986).
12. C. T. Hsu, P. Cheng and G. M. Homsy, Instability of free convection flow over a horizontal impermeable surface in a porous medium, *Int. J. Heat Mass Transfer* **21**, 1221–1228 (1978).
13. C. T. Hsu and P. Cheng, Vortex instability in buoyancy-induced flow over inclined heated surfaces in porous media, *J. Heat Transfer* **101**, 660–665 (1979).
14. K. C. Cheng and Y. W. Kim, Flow visualization studies on vortex instability of natural convection flow over horizontal and slightly inclined constant-temperature plates, *J. Heat Transfer* **110**, 608–615 (1988).
15. K. Chen and M. M. Chen, Thermal instability of forced convection boundary layers, *J. Heat Transfer* **106**, 284–289 (1984).
16. J. Y. Yoo, P. Park, C. K. Choi and S. T. Ro, An analysis on the thermal instability of forced convection flow over isothermal horizontal flat plate, *Int. J. Heat Mass Transfer* **30**, 927–935 (1987).
17. H. R. Lee, T. S. Chen and B. F. Armaly, Non-parallel thermal instability of forced convection flow over a heated, non-isothermal horizontal flat plate, *Int. J. Heat Mass Transfer* **33**, 2019–2028 (1990).
18. S. L. Lee, T. S. Chen and B. F. Armaly, New finite difference solution methods for wave instability problems, *Numer. Heat Transfer* **10**, 1–18 (1986).
19. T. S. Chen, H. C. Tien and B. F. Armaly, Natural convection on horizontal, inclined, and vertical plates with variable surface temperature or heat flux, *Int. J. Heat Mass Transfer* **29**, 1465–1478 (1986).

INSTABILITE DE TOURBILLON NON PARALLELE POUR LA CONVECTION
NATURELLE SUR UN PLAN HORIZONTAL NON ISOTHERME

Résumé—On étudie l'instabilité de tourbillon d'un écoulement de couche limite laminaire en convection naturelle sur un plan horizontal à température variant selon $T_w(x) - T_\infty = Ax^n$. L'analyse est basée sur le modèle linéaire d'écoulement non parallèle dans lequel l'écoulement moyen permanent est traité en bidimensionnel et où est prise en compte la dépendance, dans le sens de l'écoulement, des fonctions d'amplitude de perturbation. Les courbes de stabilité neutre, les nombres de Grashof critiques et les nombres d'onde critiques sont présentés pour des nombres de Prandtl $0,7 \leq Pr \leq 100$ et pour des valeurs de n allant de $-1/3$ à $1,0$. Pour un nombre de Prandtl donné, l'écoulement devient plus stable lorsque n augmente. Néanmoins, les fluides à grand nombre de Prandtl sont plus instables que ceux à faible nombre de Prandtl. Les résultats de cette analyse sont comparés avec les résultats connus des analyses d'écoulement parallèle et des expériences. La variation des perturbations dans le sens de l'écoulement semble stabiliser l'écoulement.

INSTABILITÄT DER NATÜRLICHEN KONVEKTIONSSTRÖMUNG AN EINER NICHT-
ISOTHERMEN WAAGERECHTEN EBENEN PLATTE MIT NICHT-PARALLELEN WIRBELN

Zusammenfassung—Die Wirbelinstabilität einer laminaren Grenzschichtströmung bei der natürlichen Konvektion an einer waagerechten ebenen Platte mit variabler Oberflächentemperatur $T_w(x) - T_\infty = Ax^n$ wird theoretisch untersucht. Grundlage dafür bietet das lineare nicht-parallele Strömungsmodell, bei dem die stationäre Hauptströmung zweidimensional betrachtet wird. Dabei wird die Veränderung der Amplitudenfunktion der Störung in Strömungsrichtung berücksichtigt. Die Kurven neutraler Stabilität wie auch die kritische Grashof-Zahl und die kritische Wellenzahl werden für Prandtl-Zahlen $0,7 \leq Pr \leq 100$ bei Exponenten $-1/3 < n < 1,0$ präsentiert. Es zeigt sich, daß die Strömung bei einer vorgegebenen Prandtl-Zahl stabiler wird (im Sinne der Wirbelinstabilität), wenn der Exponent n ansteigt. Fluide mit großer Prandtl-Zahl erweisen sich jedoch als empfindlicher im Hinblick auf die Instabilität als Fluide mit kleiner Prandtl-Zahl. Die Ergebnisse der vorgelegten Untersuchung mit nicht-paralleler Strömung werden mit verfügbaren berechneten und gemessenen Ergebnissen für parallele Strömung verglichen. Die Variation der Störungen in Strömungsrichtung erweist sich als stabilisierend für die Strömung.

НЕУСТОЙЧИВОСТЬ ЕСТЕСТВЕННОКОНВЕКТИВНОГО ТЕЧЕНИЯ В УСЛОВИЯХ
НЕПАРАЛЛЕЛЬНОСТИ ВИХРЕЙ НАД НЕИЗОТЕРМИЧЕСКОЙ ГОРИЗОНТАЛЬНОЙ
ПЛОСКОЙ ПЛАСТИНОЙ

Аннотация—Анализируется вихревая неустойчивость ламинарного течения в пограничном слое при естественной конвекции над горизонтальной плоской пластиной с изменяющейся температурой поверхности $T_w(x) - T_\infty = Ax^n$. Анализ основан на линейной модели непараллельных потоков, в которой основное стационарное течение считается двумерным и учитывается неоднородная по потоку зависимость амплитудных функций возмущений. Приводятся нейтральные кривые устойчивости, а также критические числа Грасгофа и критические волновые числа для интервала значений числа Прандтля $0,7 \leq Pr \leq 100$ в диапазоне значений показателя степени n от $-1/3$ до 1 . Найдено, что при заданном значении числа Прандтля устойчивость течения относительно вихревых возмущений повышается по мере увеличения значения показателя степени n . Кроме того обнаружено, что устойчивость течения жидкостей с высокими числами Прандтля ниже, чем жидкостей с низкими числами Прандтля. Результаты проведенного анализа непараллельных потоков сравниваются с известными результатами анализа параллельных потоков и экспериментальными данными. Найдено, что неоднородность возмущений в потоке оказывает на него стабилизирующее действие.